Design and Construction of a Dipolar Halbach Array with a Homogeneous Field from Identical Bar Magnets: NMR Mandhalas

H. RAICH, P. BLÜMLER

Max-Planck Institute for Polymer Research, Ackermannweg 10, 55128 Mainz, Germany

ABSTRACT: Magnets of the Halbach layout are interesting for the use in mobile NMR/MRI devices. Therefore, the ideal Halbach magnet was iterated using identical bar magnets, which are positioned and oriented based on analytical equations. These configurations were simulated with two-dimensional finite-element methods. Performance factors were defined to relate field strength with homogeneity and mass. A geometry of 16 magnets provided a good compromise between performance and special requirements for the desired use to store hyperpolarized xenon. The construction of such a magnet required the design of dedicated support frames and procedures to mount them. The field strength and homogeneity in the finished magnet were measured by a Hall probe and agreed well with the simulations. The calculation and construction are described in detail and together with the tabled field values for n magnets with $n \leq 80$ may prove helpful for building similar devices, which were named NMR Mandhalas (***M***agnet ***A***rrangements for ***N***ovel ***D***iscrete ***Ha***lbach ***La***yout). Concepts Magn Reson Part B (Magn Reson Engineering) 23B: 16–25, 2004

KEY WORDS: Halbach; magic ring; yokeless permanent magnets; homogeneous magnetic field; NMR; MRI

INTRODUCTION

In recent years, the field of mobile NMR/MRI devices has received increasing interest (*1*, *2*), and several important applications have been suggested and realized. The main problem in building portable NMR equipment is not so much the production of high magnetic fields, but rather high and homogeneous fields in a large and accessible volume.

To this end, the Halbach magnet layout (*3*, *4*) offers a unique and elegant solution to strong and homogeneous magnets. Such magnet designs are also known as "magic rings" or "magic spheres," and their field characteristics can vary from the homogeneous case, of an "inner" dipole, to that with multipoles (see Fig. 1 and theory section). The latter have applications as brushless, linear, and even spherical AC motors as well as magnetic bearings for various applications (*5*).

For NMR/MRI in moderately homogeneous fields, only the inner dipole [Fig. 1(b)] is of practical interest. The field strength being given by $B = B_r \ln r_{\text{outer}}/r_{\text{inner}}$ (*6*, *7*), where B_r is the remanence of the used magnetic material. Although in principle, arbitrarily strong magnetic fields could be achieved this way, the coercivity limits the possible strength to values around 3–4 T (*8*). However, the slow increase in flux, which varies with the logarithm of the ratio of the outer and inner radius of the "magic ring" makes a direct scaling impractical due to the large resulting mass of such a magnet. Hence, various approaches to

Received 25 March 2004; revised 27 May 2004; accepted 1 June 2004

Correspondence to: P. Blümler; E-mail: bluemler@mpip-mainz.mpg.de

Concepts in Magnetic Resonance Part B (Magnetic Resonance Engineering), Vol. 23B(1) 16–25 (2004)

Published online in Wiley InterScience (www.interscience.wiley.com). DOI 10.1002/cmr.b.20018

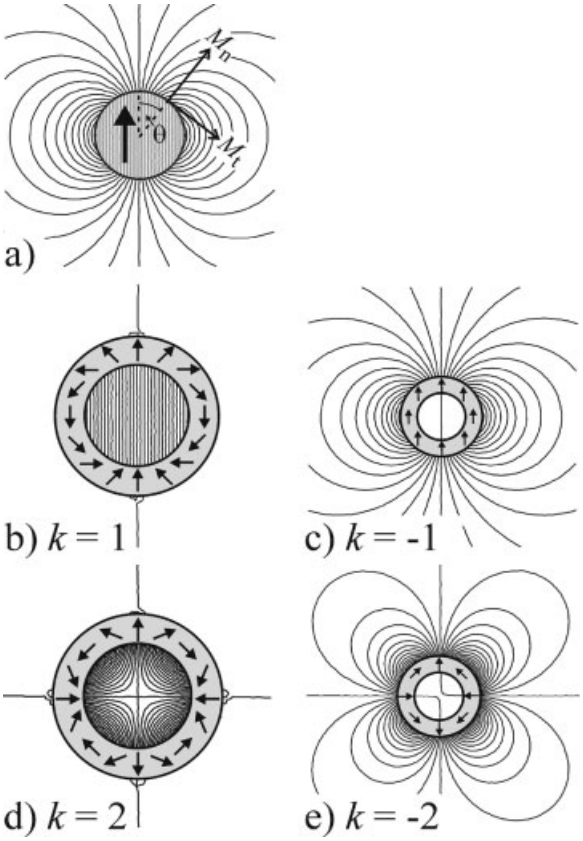

Figure 1 Explanation of the Halbach geometry according to Eqs. [1] and [2]: (a) Magnetic flux inside and around a homogeneously magnetized cylinder. The axes illustrate the normal, M_n, and tangential, M_t, magnetization directions. The graphs illustrate the field of a dipolar Halbach array with flux inside (b) and outside (c) as well as a quadrupolar Halbach array with flux inside (d) and outside (e). Arrows indicate the magnetization direction.

increase the flux by use of additional rings (*8*) or iron inserts (*6*) have been proposed.

This work is a continuation of earlier attempts to split this principal design into many pieces in order to lower the weight of the arrangement (*7*, *9*). This will of course lower the density, but not necessarily the homogeneity, of the magnetic flux. Furthermore, the arrangement should be assembled from bar magnets of identical size to minimize production costs and simplify construction. This is also of importance for the improvement of the homogeneity, because the individually polarized segments of an annular structure, as seen in Fig. 1, are difficult to produce and are a major source of field variations.

Although we needed such a magnet for a different application (storage of hyperpolarized xenon), the main task was to produce magnets of a robust design and to evaluate their properties. A simple design scheme allowed for the simulation of Halbach magnet arrays produced from n identical bar-shaped magnets (square cross section). This type of design was named "NMR Mandhala" (**M**agnet **A**rrangements for **N**ovel **D**iscrete **Ha**lbach **La**yout from Tibetan for a round symbol, "that which encircles a center," and a Buddhist symbol for wholeness, unity, and harmony).

Specially for NMR/MRI applications, devices of this layout have the following advantages:

- high homogeneity
- close to optimum use of mounted magnetization
- transverse field direction (allows the use of solenoidal coils for NMR)
- very small stray field
- made from identical, simple magnets
- robust
- easy and cheap to produce

THEORY

A detailed theoretical description of permanent magnetic materials can be found elsewhere (*10*).

The flux on the surface of a circle, or cylinder containing an homogeneous field, is given by the polar coordinates

$$\mathbf{M} := \begin{pmatrix} M_t \\ M_n \end{pmatrix} = M_0 \begin{pmatrix} \sin\theta \\ \cos\theta \end{pmatrix} \quad \text{with } \theta = 0 \ldots 2\pi. \qquad [1]$$

with M_t the tangential and M_n the normal component [see Fig. 1(a)].

To mimic these field characteristics inside a hollow cylinder made from discrete magnetic parts, the magnetization direction in the i^{th} magnet has to be (see Fig. 2) (*5*)

$$\gamma_i := (1 + k)\beta_i \quad \text{with } k \in \mathbb{Z} \quad \text{and} \quad i = 0, 1, \ldots, n-1 \qquad [2]$$

where k is the number of pole-pairs or modes (i.e., $k = \pm 1$ for a dipolar, $k = \pm 2$ for a quadrupolar field). The sign in the angular component, k, directs the flux inside ("+") or outside ("−") the Halbach magnet [see Fig. 1(b–e)].

NMR engineers are aware of this principle in the context of homogeneous, transverse rf fields (B_1 fields) as used in saddle coils and birdcages and their modes (*11*). Hence, for the envisaged concept of homogeneous flux inside the magnet ring, $k = +1$ is

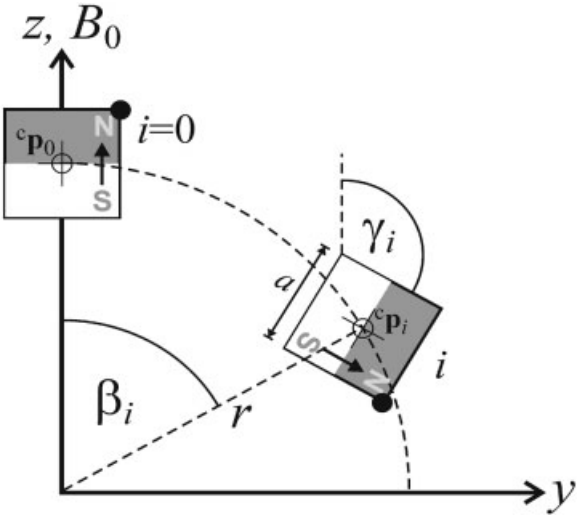

Figure 2 Schematic geometry of magnet coordinates and illustration of the symbols used. The corner with index 1 is marked by a full dot and the centers of each magnet by crosshairs.

the value of choice [see Fig. 1(b)]. Such arrays are also known as "magic rings" (*6*, *8*, *12*).

DESIGN

The construction principle is illustrated in Fig. 2. For the calculation of the exact geometry of the magnet arrangement, only two parameters are predetermined: the radius of the ring, r, and the number of magnets, n. Each magnet is positioned such, that its center (vector ${}^{c}\mathbf{p}_i$) has the same distance r from the origin. The coordinates of each magnet center are then

$$ {}^{c}\mathbf{p}_i := \begin{pmatrix} {}^{c}y_i \\ {}^{c}z_i \end{pmatrix} = r \begin{pmatrix} \sin\beta_i \\ \cos\beta_i \end{pmatrix} $$

$$ \text{with } \beta_i := i\alpha \quad \text{for } i = 0, 1, \ldots, n-1 $$

$$ \text{and} \quad \alpha := \frac{2\pi}{n} \qquad [3] $$

where β_i is the angle between the i^{th} magnet center and the direction of the main field, B_0 (by definition, the z axis; see Fig. 2). The orientation of the i^{th} magnet relative to the z axis is then given by the angle $\gamma_i = 2\beta_i$ (see Eq. [2]). Once the n magnets are spatially arranged (calculating $n/8$ magnets or one octant is sufficient due to symmetry), their size, a, is scaled such that the most dense arrangement results.

This gives the following coordinates of each corner of the i^{th} bar-magnet

$$ {}^{1}\mathbf{p}_i := \begin{pmatrix} {}^{1}y_i \\ {}^{1}z_i \end{pmatrix} = {}^{c}\mathbf{p}_i + \frac{a}{\sqrt{2}} \begin{pmatrix} \cos\xi_i \\ \sin\xi_i \end{pmatrix} $$

$$ {}^{2}\mathbf{p}_i := \begin{pmatrix} {}^{2}y_i \\ {}^{2}z_i \end{pmatrix} = {}^{c}\mathbf{p}_i + \frac{a}{\sqrt{2}} \begin{pmatrix} -\sin\xi_i \\ \cos\xi_i \end{pmatrix} $$

$$ {}^{3}\mathbf{p}_i := \begin{pmatrix} {}^{3}y_i \\ {}^{3}z_i \end{pmatrix} = {}^{c}\mathbf{p}_i + \frac{a}{\sqrt{2}} \begin{pmatrix} -\cos\xi_i \\ -\sin\xi_i \end{pmatrix} $$

$$ {}^{4}\mathbf{p}_i := \begin{pmatrix} {}^{4}y_i \\ {}^{4}z_i \end{pmatrix} = {}^{c}\mathbf{p}_i + \frac{a}{\sqrt{2}} \begin{pmatrix} \sin\xi_i \\ -\cos\xi_i \end{pmatrix} $$

$$ \text{with } \xi_i := \frac{\pi}{4} - 2\beta_i \qquad [4] $$

Here each corner is represented by a vector ${}^{j}\mathbf{p}_i$, where the index i identifies the magnet and j denotes the corner, numbered in the sense of quadrants as shown in Fig. 3. The length of a magnet's side, a, is found by solving ${}^{4}\mathbf{p}_{\frac{n}{8}-1} + \lambda({}^{1}\mathbf{p}_{\frac{n}{8}-1} - {}^{4}\mathbf{p}_{\frac{n}{8}-1}) = {}^{3}\mathbf{p}_{\frac{n}{8}}$, which gives

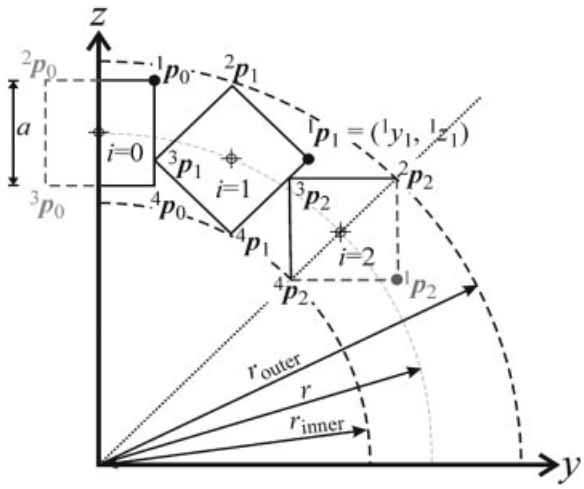

Figure 3 Schematic representation of the magnet coordinates. The positions of the first three magnets (i = 0, 1, 2 for $n = 16$) are shown. The nomenclature of the corner indices and radii is illustrated.

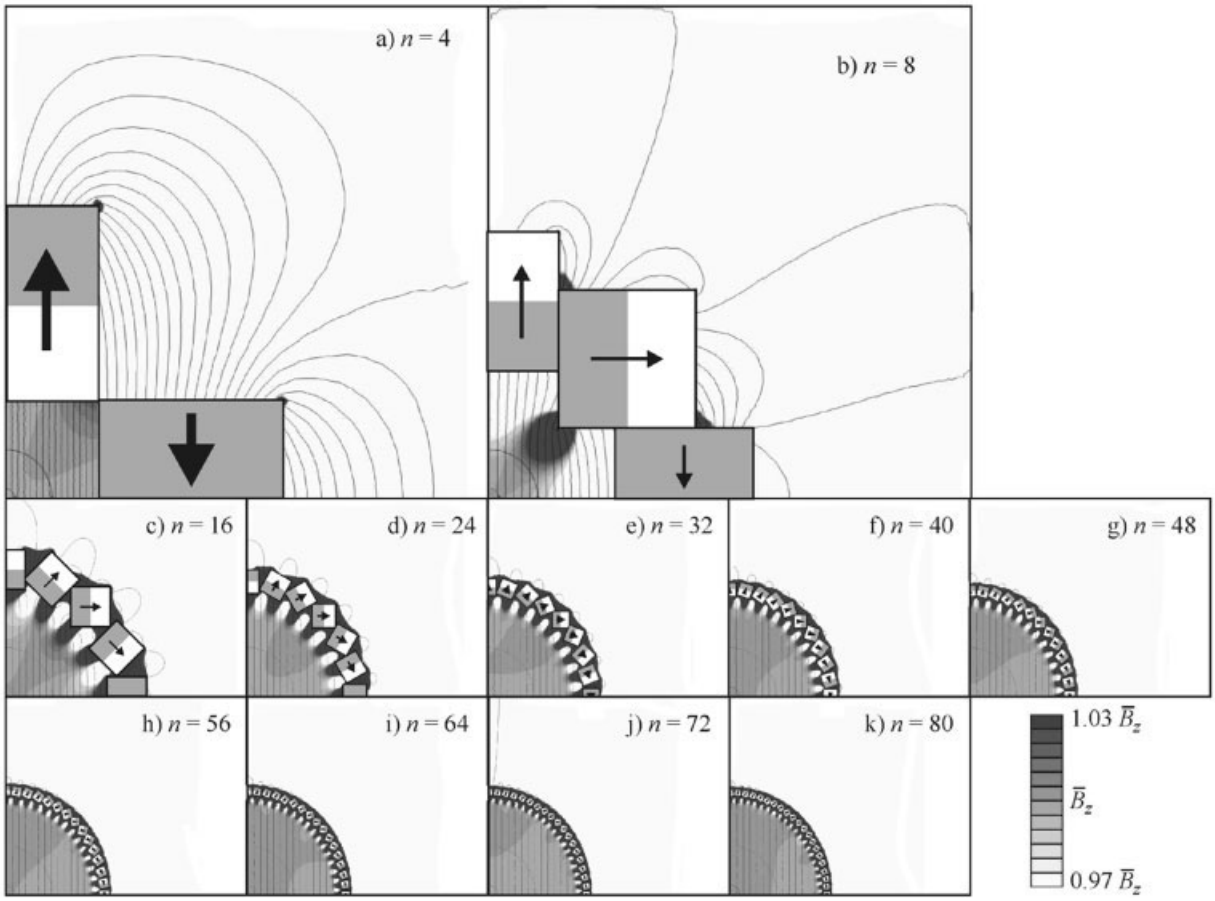

Figure 4 Results of the finite element simulation for various n and identical r_{inner}. Due to the inherent symmetry, only the first quadrant of the Halbach rings is shown at the same spatial scale. Nineteen field lines are used to illustrate the homogeneity and cancellation of the stray field. The grey scale ranges from 97% to 103% of the flux in the center. (a) $n = 4$, (b) $n = 8$, (c) $n = 16$, (d) $n = 24$, (e) $n = 32$, (f) $n = 40$, (g) $n = 48$, (h) $n = 56$, (i) $n = 64$, (j) $n = 72$, and (k) $n = 80$.

$$a = 2r\Xi(\alpha)$$

$$\text{with } \Xi(\alpha) := \frac{\cos\alpha - \sin\alpha - \sqrt{2}\sin\left(\frac{\pi}{4} - 2\alpha\right)}{2\cos\left(\frac{\pi}{4} - 2\alpha\right) + \sqrt{2}} \quad [5]$$

Hence, the area, A, occupied by the n magnets is

$$A = na^2 = 4nr^2\Xi(\alpha)^2 \quad [6]$$

The inner radius (accessible for experiments) is then given by

$$r_{\text{inner}} = r\,(1 - \sqrt{2}\,\Xi(\alpha)) \quad [7]$$

and the radius of the outer perimeter is

$$r_{\text{outer}} = r\,(1 + \sqrt{2}\,\Xi(\alpha)) \quad [8]$$

SIMULATION

The finite element simulations of the different arrangements were performed in the 2D-freeware package FEMM 3.3 (David Meeker, Foster-Miller, Inc., Waltham, MA). The geometry input files of FEMM were created by a MATLAB script (MathWorks, Inc.), which computes Eqs. [3–8]. These are then meshed and solved by FEMM with a numerical precision of 10^{-8}. The number of mesh-nodes turned out to be most critical for the simulated homogeneity. Therefore, the most complex design ($n = 80$) was simulated with different numbers of finite elements and the homogeneity analyzed. An asymptotic behaviour was observed, where an accuracy of 95% of the asymptotic value was chosen as

Table 1 Summary of the Geometrical Properties for Various Numbers of Magnets (n, at r_{inner} = 50 mm)

n	r (mm)	r_{outer} (mm)	a (mm)	A (cm^2)	$\bar{B}_z(r_1, r_2)$ (T)	$\Delta B_z(r_1)$ (ppm)	$\Delta B_z(r_2)$ (ppm)	ω (MHz)	m[a] (kg)
4	100	150	100	400	.723	105	.883	30.550	75.20
8	100	150	70.7107	400	.777	3395	20.9	32.813	75.20
16	64.4472	78.8943	20.4314	66.7906	.311	800	9.33	13.141	12.56
24	58.4220	66.8440	11.9105	34.0464	.193	235	5.22	8.149	6.40
32	55.9285	61.8570	8.3842	22.4941	.139	107	3.23	5.866	4.23
40	54.5685	59.1370	6.4608	16.6969	.108	63.9	2.22	4.579	3.14
48	53.7136	57.4272	5.2518	13.2391	.0890	44.6	1.64	3.742	2.49
56	53.1270	56.2541	4.4223	10.9517	.0750	33.9	1.28	3.166	2.06
64	52.6999	55.3998	3.8182	9.3303	.0648	27.46	1.05	2.729	1.75
72	52.3750	54.7501	3.3588	8.1228	.0570	22.58	.866	2.402	1.53
80	52.1198	54.2396	2.9978	7.1896	.0510	19.46	.756	2.149	1.35

[The results of the simulations are the average flux, $\bar{B}_z(r)$, and its homogeneity, $\Delta B_z(r)$, for two different areas ($r_1 \leq 25$ mm and $r_2 \leq 5$ mm), the NMR frequency, ω, for ^{1}H, and the mass, m.]

[a] For $h = 250$ mm without support materials and $\rho = 7.52$ g/cm^3.

a sufficient compromise between runtime and precision. This corresponds to a number of mesh-nodes around 10^6. The magnetic material was assumed to be FeNdB-37 (permeability $\mu = 1.049$, coercivity $H_c = 911$ kA/m, assuming a linear B vs. H dependence. The magnetic properties of the material in the simulation was fine-tuned in accordance with the obtained field measurements for the $n = 16$ array.) Halbach arrays made from $n = 4, 8, 16, 24, \ldots 80$ magnets were simulated for the same inner radius ($r_{inner} = 50$ mm). The results are depicted in Fig. 4.

To analyze the data, the results were read into MATLAB and interpolated onto a Cartesian grid. Averages and standard deviations of the local magnetic flux were computed from such equally spaced data. This was done for two areas, one with a radius of $r_1 := 0.5\, r_{inner}$ and another of $r_2 := 0.1\, r_{inner}$. Table 1 lists the results obtained from these procedures. The results should be invariant to the spatial scaling of the problem, and hence can be used to quickly estimate the magnetic flux and mass of the desired geometry.

To quantify the performance of the simulated magnet arrays, a field-performance factor,

$$f_B(r) = \frac{\bar{B}_z(r)}{\Delta B_z(r)} \qquad [9]$$

is defined by dividing the average field by the inhomogeneity, such that f_B is high for strong fields and high homogeneity. Figure 5(a) shows this performance factor for the simulated arrays. A distinct maximum at $n = 4$ is observed, but this array is definitely too bulky for most applications [see Fig. 4(a) and Table 1]. Therefore, a second performance factor, f_A, is defined which relates f_B to the area of the magnets, which is thus proportional to the mass of the structure. Consequently, f_A is increasing for high fields, high homogeneity, and low weight.

$$f_A(r) = \frac{\bar{B}_z(r)}{\Delta B_z(r)\, A} \qquad [10]$$

The dependence of $f_A$on the number of magnets is shown in Fig. 5(b). Now it becomes clear that performance of the $n = 4$ array is exceeded by $n = 24$ or 48, depending on the analysed volume. Figure 5(b) also shows that there is an asymptotic value of the performance for large n, and that the improvement is more significant for larger volumes.

However, the property of interest in an NMR experiment is the sensitivity, which scales with Larmor frequency to the $(7/4)^{th}$ power (*13*). Hence, a third performance factor is defined to take this into account.

$$f_\omega(r) = \frac{\omega^{\frac{7}{4}}}{\Delta B_z(r)\, A} = \frac{(\gamma \bar{B}_z(r))^{\frac{7}{4}}}{\Delta B_z(r)\, A} \qquad [11]$$

This performance factor is shown in Fig. 5(c). Here the maximum stays at $n = 4$ for small volumes in the center, which could be of importance for spectroscopic setups using microcoils.

CONSTRUCTION

For the desired application, the magnet should have a B_0 of at least 0.2 T (at a reasonable homogeneity of

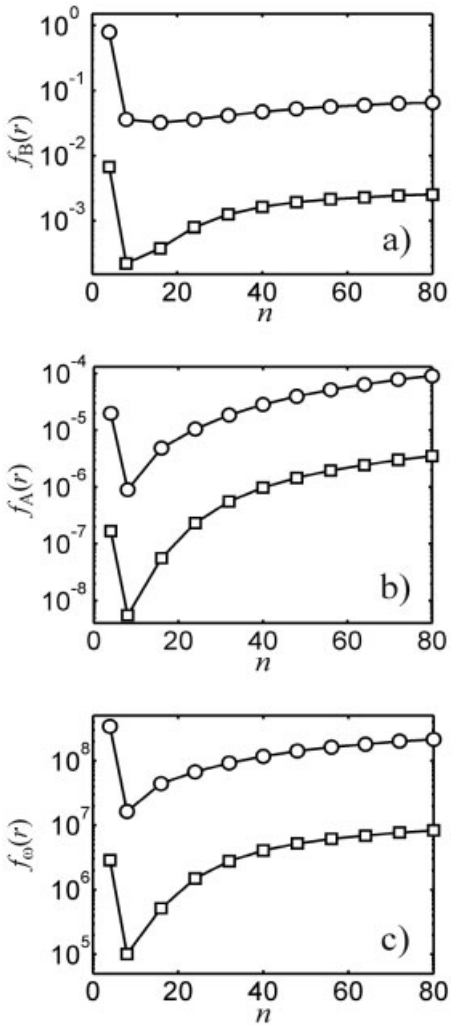

Figure 5 Semilogarithmic plot of the performance factors of the simulated properties of the magnets versus n: (a) f_B according to Eq. [9], (b) f_A according to Eq. [10], (c) f_ω according to Eq. [11]. Squares for $r_1 \leq 25$ mm and circles for average over area with $r_2 \leq 5$ mm. Lines are guides for the eye only.

ca. 1% over a central volume of 1 cm^3) to separate the resonances of ^{129}Xe and ^{131}Xe sufficiently. Therefore, a compromise between field strength and homogeneity had to be made, and it was decided to build an array with 16 magnets. Additionally, the resulting ring had to surround a Dewar flask with an outer diameter of 70 mm. All this resulted in the following geometry, calculated from Eqs. [4–8]: $r = 56.78$ mm, $a = 18$ mm, $A = 51.84$ cm^2, $r_{inner} = 44.04$ mm, and $r_{outer} = 69.51$ mm.

According to these values permanent magnets, made from sintered FeNdB Grade 45 (N-45) and coated with nickel, were ordered from Ningbo Ninggang Permanent Magnet Element Factory (Yinxian Ningbo, People's Republic of China). These magnets had dimensions of $18 \times 18 \times 27$ mm^3, with a mechanical tolerance of about ± 0.1 mm and a density of $\rho = 7.52$ g/cm^3. The magnets were chosen to be relatively short in the third dimension, so that they can still be manipulated without special tools and safety precautions. The manufacturer specified the following magnetic properties for these permanent magnets: remanence $B_r = 1.33$–1.37 T, coercivity $H_c = 836$–876 kA/m, and a maximum energy product $(BH)_{max}$ of 43–45 MGOe.

To mount the magnets in the correct position and orientation, a supporting structure needed to be designed that was robust enough to withstand the strong mutual forces of the bar magnets. For this purpose, 6-mm aluminium disks were fabricated by a computer-controlled milling cutter [see Fig. 6(a)]. The mounting process of individual magnets is shown in

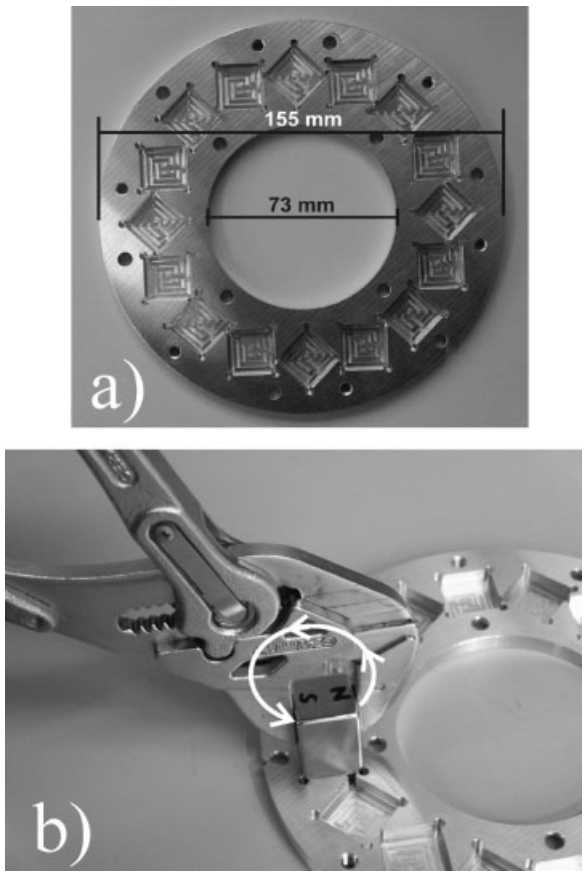

Figure 6 (a) Support ring showing the 16 5.7-mm deep sockets for the magnets. They were milled out from 6-mm sheet aluminium. The depths of the sockets were 5.7 mm. The "spiral" structure on the bottom of each socket is merely the path of the milling tool. (b) Magnetic "shorting" of a magnet by the use of a pair of ferromagnetic pliers.

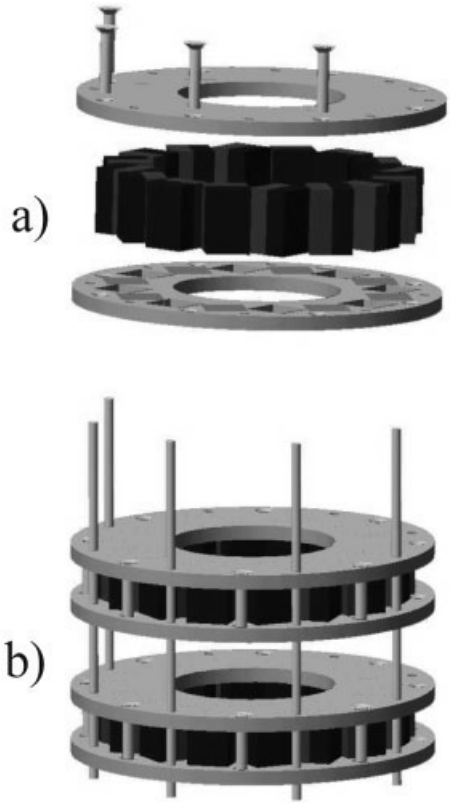

Figure 7 Schematic rendering of the supporting structure. (a) Exploded view of the magnets (dark in the center) being mounted between a top and bottom support ring and fixed by bolts. (b) Assembly of two "sandwich" subunits from (a) to a stacked magnet using threaded rods resulting in a separation of 0.6 mm between the magnets in adjacent stacks.

Fig. 6(b) where a heavy pair of ferromagnetic pliers was used to "short" the magnetic flux. This was useful in the completion of the array, with the last magnets being strongly repelled. Once brought in position, the magnets were glued into their individual sockets. A second support ring, or top piece, was used to hold the magnets in the desired positions during the curing of the glue.

The inner faces of the top and bottom support rings are identical in terms of the sockets for the magnets; however, they differ on the outer faces, with holes for nuts and bolts. This complication became necessary because each layer of magnets, sandwiched between such a top and bottom support piece, needed to be fixed by brass bolts [see Fig. 7(a)]. These "sandwiches" were then stacked on threaded brass rods and forced together by nuts [Fig 7(b)].

While the flux at the center of one of these sandwiches is about 0.1 T, the process of forcing them into a stack significantly increases the flux density, until a maximum of 0.311 T was reached in the center of a stack of eight subunits. Figure 8 shows a single bar magnet, a finished "sandwich," and the final Halbach magnet used in our lab made from a stack of eight sandwich subunits. This final magnet had a mass of 11.4 kg (8.4 kg magnet material and 3 kg aluminium and brass).

FIELD MEASUREMENT

The magnetic field in the constructed magnet was scanned using a home-built device, to move a Hall sensor across the sample via an xy table. A computer controls the positioning and records the values from a Gaussmeter 420 (Lakeshore Cryotronics, Inc.). With this setup, the z and y components of the magnetic field were scanned across an area of 40×40 mm^2 in the central plane ($x = 0$). Additionally the z component was measured along the axis of the magnet ($y = z = 0$). The results are summarized in Fig. 9. Unfortunately, the z component was in the order of 0.3 T and directly at a switching value of the range of the used Gaussmeter. Therefore, the achieved precision was limited to 0.1 mT for the z component, which is in the same range as the inhomogeneities. This can be seen in the distinct levels in Fig. 9(f). Otherwise, the agreement between simulation and measurement is impressive, considering that only a two-dimensional FEM simulation was carried out.

The standard deviation between measured and simulated fields was determined similarly to that of the simulations for an area with a radius of 20 mm (slightly smaller than r_1 in Table 1). The values were $\sigma_y = 5.4 \cdot 10^{-3}$ T and $\sigma_z = 7.8 \cdot 10^{-4}$ T (2500 ppm) and thus about a factor of about 3 worse than the predicted 800 ppm (see Table 1). With a maximum value of 3.5 mT, the y component is in a comparable range. Of course the inhomogeneity of B_z in the yz plane increases with x deviating from 0 [as shown in Fig. 9(a)]. However, for a sphere in the center with a radius of 10 mm the field doesn't change within the sensitivity limits of the used Gaussmeter.

Looking at a greater distance along x, of course, worsens the homogeneity, reaching a gradient strength of roughly 0.3 T/m over the scanned range [see Fig. 9(b)]. However, the homogeneity in this direction can easily be improved by adding more "sandwiches" to the stack.

In summary, in a volume of $5 \times 5 \times 5$ mm^3, the homogeneity is better than 0.1 mT, which is the limiting sensitivity of the Hall probe used at a field strength of 0.311 T. In a first NMR experiment at a ^{1}H

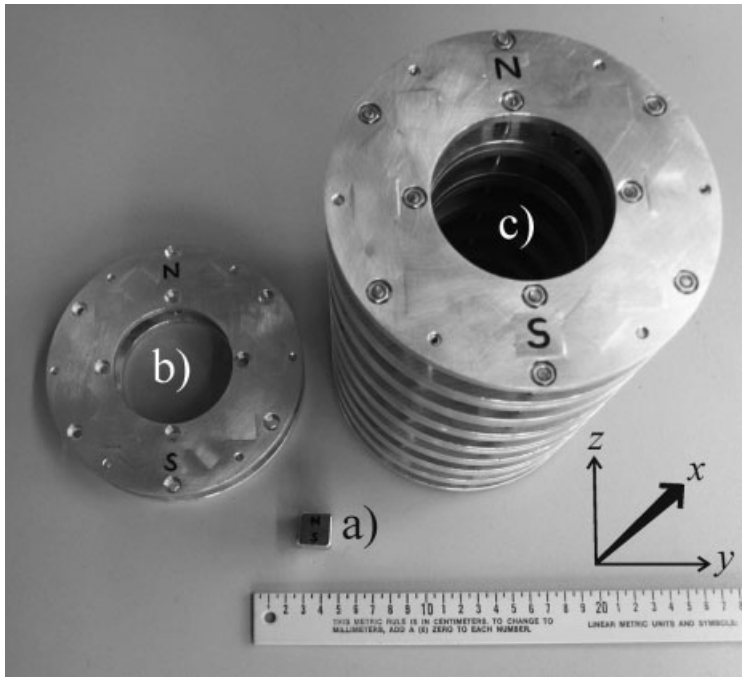

Figure 8 Photograph of (a) a single bar-magnet, (b) a finished "sandwich" subunit, and (c) the final magnet made from a stack of eight "sandwich" subunits. The right-handed axes are for illustration of the nomenclature.

frequency of 12.8 MHz, a line width of ~9 kHz (700 ppm) was observed for a $18 \times 18 \times 30$ mm^3 (x, y, z) water sample, which is in good agreement with the simulated 800 ppm for a slightly larger area in Table 1. However, the same measurement also revealed a very broad peak (~5000–7000 ppm) of lower intensity, which is very likely to be caused by protons further away from the center (S. Anferova, V. Anferov, private communication). Future MRI experiments will give more precise values.

DISCUSSION

From the simulations it becomes clear that the maximum field strength is achieved with a small number of bulky magnets. However, it is questionable that such geometries will be used in mobile NMR because of the high mass in comparison to relatively small accessible volumes. Therefore, performance factors were defined in Eqs. [9–11] where the field strength was related to homogeneity, mass, and NMR sensitivity. From Table 1 and Fig. 5 it can be seen that it depends on the special needs of an application to define an optimal number of magnets. The asymptotic behavior observed in Fig. 5 is somewhat unrealistic, because the inhomogeneities will increase due to the higher tolerances in manufacturing smaller magnets. However, it is difficult to give a value for such a trade-off, because manufacturing tolerances will depend on the size of the object. A good overview about the achievable field strengths and homogeneities is given in Table 1. Because these parameters should be independent of the scale of the design, the desired choice can be directly picked from this table or tailored to the needed field strength by using magnets with different remanences.

The acquired spectra of bulk samples cannot easily be used to determine the homogeneity, because they might overemphasize the signal from the homogeneous center (a problem that could be solved by future localized NMR measurements). Therefore, field measurements performed by a Hall probe are given preference, although the observed inhomogeneities (see Fig. 9) differ by a factor of 3 from the prediction. Various problems could cause such deviations. First, the accuracy in manufacturing was relatively low (in the percent range). Although the deviation in the magnetization direction is greatly reduced by using bar magnets, there are still large variations in the remanence (± 0.2 T) and size (± 0.1 mm). Additionally, the sintered FeNdB material by itself can be quite inhomogeneous on a millimeter level. Mounting the magnets might also locally reduce the magnetization due to unavoid-

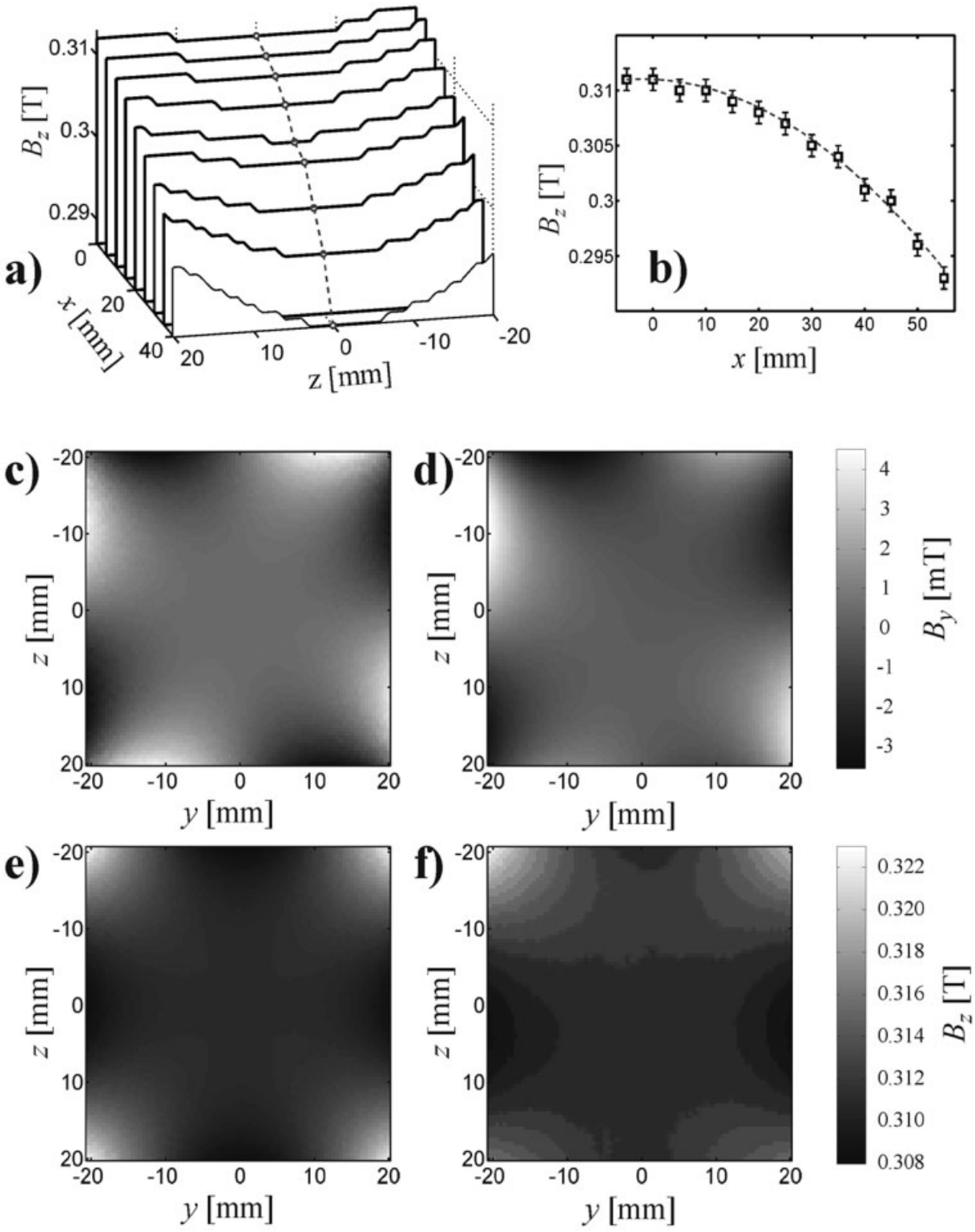

Figure 9 Comparison of measured and simulated magnetic flux density: (a) measured B_z in the xz plane ($y = 0$). The dashed line connects the central points, which were measured separately using smaller steps as shown in (b) B_z along the array axis, x. The dashed line is a fit of the data by a quadratic polynomial. (c, d) $B_y(y,z)$ in the center ($x = 0$) of the array (c) simulation and (d) measurement; (e, f) $B_z(y,z)$ in the center ($x = 0$) of the array (e) simulation and (f) measurement. Note: the scale for (c) and (d) is in mT.

able impacts. Finally, the temperature coefficient for FeNdB is large ($\sim$ 0.1% of the remanence per Kelvin), so that keeping the whole assembly at uniform temperatures might be more demanding than the mechanical design.

Different ideas of shimming Halbach magnets, by addition of a second magnetic ring (*8*, *12*, *14*), are already discussed but would add tremendously to the mass.

CONCLUSIONS

The design principle and simulation of Halbach magnets formed by iteration with n bar magnets was demonstrated. The optimization for mobile NMR/MRI devices was achieved by introducing performance factors, which combine field strength and homogeneity with the mass of the device or the NMR signal strength. However, due to special needs, a compromise of $n = 16$ was built and tested. A good agreement between simulated and measured field values was found, showing that the properties listed in Table 1, for various designs, seem reliable and may be useful as a reference.

The results are promising for NMR experiments in moderately homogeneous fields (e.g., measurements of relaxation times, diffusion coefficients, and porosity), which might greatly benefit from a portable and self-shielded magnet design. Future work will focus on the development of resistive shim and gradient coils for this special geometry.

ACKNOWLEDGMENTS

We thank K. Kupferschläger, V. Anferov, and B. Blümich (ITMC, RWTH-Aachen) for allowing access to their field scanner. S. Hiebel (Insitut für Physik, University of Mainz) is thanked for finding some inconsistencies in the original manuscript. At the MPI for Polymer Research we thank M. Hehn and F. Keller for their help in the construction, T. Runkel for manufacturing the support rings, M. Parkinson for carefully checking the manuscript, and H.W. Spiess for giving access to all the toys and tools. Special gratitude goes to Silvia Schleidt for the suggestion of the name "NMR Mandhala." Finally, the authors are indebted to Eiichi Fukushima (New Mexico Resonance, Albuquerque, New Mexico) for helpful discussions and pointing our ignorant views to other people's work. We also appreciate the helpful suggestions of an anonymous referee.

REFERENCES

1. Eidmann G, Savelsberg R, Blümler P, Blümich B. 1996. The NMR MOUSE, a mobile universal surface explorer. J Magn Reson A 122:104–109.
2. Blümich B. 2000. NMR imaging of materials. Oxford: Clarendon Press.
3. Halbach K. 1979. Strong rare earth cobalt quadrupoles. IEEE Trans Nucl Sci 26(*3*):3882–3884.
4. Halbach K. 1980. Design of permanent multipole magnets with oriented rare earth cobalt materials. Nucl Instr Meth 169:1–10.
5. Zhu ZQ, Howe D. 2001. Halbach permanent magnet machines and applications: a review. IEE Proc Eng Power Appl 148:299–308.
6. Leupold HA, Tilak AS, Potenziani E II. 1993. Multitesla permanent magnet field sources. J Appl Phys 73:6861–6863.
7. Moresi G, Magin R. 2003. Miniature permanent magnet for table-top NMR. Concepts Magn Reson B 19:35–43.
8. Leupold HA, Tilak AS, Potenziani E II. 1993. Adjustable multi-tesla permanent magnet field sources. IEEE Trans Magn 29:2902–2904.
9. MAGNETICASOFT, Nice, France: MRI Halbach 0.23 T magnet available at: http://www.magneticasoft.com/magnetdesign/magnet2.html
10. Campbell P. 1996. Permanent magnet materials and their application. Cambridge: Cambridge University Press.
11. Jin J. 1999. Electromagnetic analysis and design in magnetic resonance imaging. Boca Raton, FL: CRC Press.
12. Abele MG, Chandra R, Rusinek H, Leupold HA, Potenziani E. 1989. Compensation of non-uniform magnetic properties of components of a yokeless permanent magnet. IEEE Trans Magn 25:3904–3906.
13. Callaghan PT. 1991. Principles of nuclear magnetic resonance microscopy. Oxford: Clarendon Press p 178.
14. Bertora F, Trequattrini A, Abele MG, Rusinek H. 1993. Shimming of yokeless permanent magnets designed to generate uniform fields. J Appl Phys 73:6864–6866.